Effects of thermal stratification on detonation development in hypersonic reactive flows

Pengfei Yang [1,2] Dehai Yu [1,2] Zheng Chen [2] Honghui Teng [3,*] and Hoi Dick Ng [4]

[1]*State Key Laboratory of High Temperature Gas Dynamics, Institute of Mechanics, Chinese Academy of Sciences, Beijing 100190, China*
[2]*College of Engineering, Peking University, Beijing 100871, China*
[3]*School of Aerospace Engineering, Beijing Institute of Technology, Beijing 100081, China*
[4]*Department of Mechanical, Industrial and Aerospace Engineering, Concordia University, Montreal, Quebec, Canada H3G 1M8*

Gaseous detonation waves in a uniform mixture have been studied widely, but uniformity is seldom realized in practical applications such as detonation-based engines. Nonideal scenarios involving incomplete mixing and curved intake compression lead to the thermal stratification of reactants. Local high-temperature regions first trigger the reactant autoignition and even result in the untimely formation of a detonation wave. Using the two-dimensional Euler equations and a detailed H_2–air reaction mechanism, we examine the effects of reactant thermal stratification on the autoignition wave morphology in hypersonic reactive flows. Three flow regimes, namely, the autoignition-driven reaction front, detonation wave, and decoupling shock/reaction front, are observed. These flow regimes are determined by the temperature gradient, and only a moderate temperature gradient can trigger an oblique detonation wave. The oblique detonation can stabilize in hypersonic inflows, primarily because the upstream autoignition region acts as an anchorage point. Comparisons of one- and two-dimensional autoignitions confirm that supersonic flow enhances the formation of pressure waves. An analysis of the reaction front propagation speeds reveals that the detonation development is determined by two aspects. One is the convergence of compression waves originating from thermal expansion and supersonic flows, and another is the reaction front propagation speed at the early stage, which must exceed the local sound speed to promote positive feedback between pressure waves and heat release.

I. INTRODUCTION

The gaseous detonation wave is characterized by a strong shock wave followed by a chemical reaction zone, where the heat release increases the temperature, sustaining the propagation of the leading shock. In a gaseous mixture, the detonation waves propagate at a constant supersonic speed. Because of high thermal efficiency and rapid reaction, detonation waves have gained increasing attention for hypersonic propulsion in recent years [1–4]. Nonetheless, challenges persist in harnessing the advantages of detonation waves in combustors owing to nonideal operating conditions.

Ideally, the gaseous detonation wave is a premixed combustion mode, meaning the fuel and oxidizer must be thoroughly mixed at the molecular level prior to combustion. One of the main challenges in detonation propulsion is creating a premixed mixture. In practical engines, the flow,

---

*Contact author: hhteng@bit.edu.cn

constrained by the combustor walls, may cause the spatial variations in thermodynamic states, resulting in nonuniform reactivity of the premixed mixture. Such nonuniformity in reaction rate can affect autoignition characteristics, potentially causing the formation of an undesired detonation.

According to the Arrhenius reaction law, the temperature is of pivotal importance in determining the reaction rate of the combustible mixture. Temperature nonuniformity, characterized by local hot spots [5], plays a prominent role in affecting the formation of autoignition waves. Autoignition occurs in a high-temperature region and then transforms into an outwardly propagating reaction front [6–9]. Zel'dovich [10] observed the scaling relation between the reaction front's propagation speed u_f and the combustible mixture's reactivity, i.e., $u_f \sim (\nabla \tau_{ig})^{-1}$, where τ_{ig} is the autoignition delay time. Depending on the magnitude of u_f, the reaction front can be classified as a laminar burning deflagration, slow autoignition deflagration, rapid autoignition deflagration, or developing detonation. The transition from autoignition to detonation can be interpreted through a theoretical criterion by comparing the propagation speeds of the reaction front and the acoustic wave [11–14]. These findings demonstrate that the presence of a temperature nonuniformity in the flow field can affect the initiation and propagation of the detonation waves.

Temperature nonuniformity in direct-injection gasoline engines may precipitate the superknock phenomenon, which can be regarded as the detonation initiation in a static mixture [14]. Autoignition response time can extend to several hundreds of microseconds, potentially triggering a detonation wave. Moreover, the critical temperature gradients that induce detonation in such static surroundings are, in general, lower than 1.0 K/mm [6–9]. This scenario contrasts sharply with the conditions in hypersonic air-breathing engines, where the interactions between the fuel jet and hypersonic airstream affect the temperature distribution [15,16]. In these engines, the thermal boundary layer may further intensify the temperature nonuniformity within the reacting flow, for instance the local temperature gradient can exceed 15.0 K/mm [2,17]. As the hypersonic airstream passes through the combustion chamber, it interacts with the ensuing reaction front. This leads to a series of compression waves [18–20], producing complex temperature nonuniformities in the reactive flow. These temperature nonuniformities can influence the detonation/autoignition behavior under hypersonic flows. Yet the underlying mechanisms remain to be elucidated, which motivates this study.

Considering the temperature distributions of hypersonic reactive flows, this paper aims to explore two aspects. The first objective is to investigate the morphology of autoignition waves triggered by varying temperature profiles and assess the occurrence of detonation. The second objective focuses on the effects of hypersonic flows on detonation development induced by thermal stratification. We discuss the dependence of wave morphology on the reactant temperature gradient and systematically examine the critical temperature profiles for detonation development. Using simplified models, we further analyze the interaction between the supersonic flow and the reaction front, shedding light on pressure wave formation. Finally, we analyze the propagation speeds of the reaction front to determine how reactant thermal stratification influences detonation development in hypersonic flows.

II. SIMULATION METHODS

A. Model description and parameters

To assess the thermal stratification effect on hypersonic reactive flows, the simplified model in Fig. 1 is used to reproduce the thermal stratification of flow fields. When the hypersonic flow travels in this channel, the mixture autoignition first occurs in the high-temperature region. Meanwhile, the local thermal expansion induced by the autoignition interacts with the hypersonic inflow, inducing a series of compression waves that further enhance the coupling of flow and heat release. In this way, shock or detonation waves probably form downstream.

Because of the problem's symmetry, simulations only take into account half of the physical model, which is shown by the blue dashed box in Fig. 1. For the computational domain (the blue
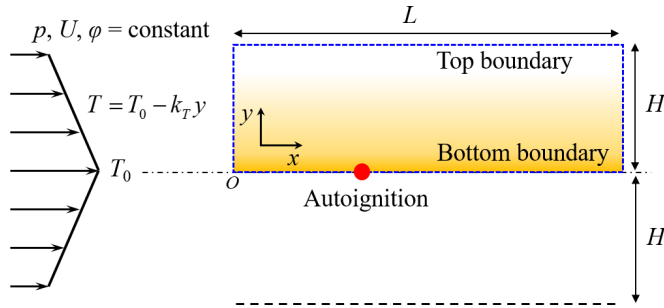
FIG. 1. Schematic of a hypersonic reactive flow with thermal stratification. The blue dashed box is the computational domain.

dashed box) in Fig. 1, the pressure p, velocity U, and equivalence ratio ϕ at the left entrance are constant owing to the characteristics of the supersonic inflow. Variables p, U, and ϕ are assumed to be uniform to reduce the complexity of the inflow. The linear temperature profile of the entrance mixture is controlled by two key parameters, namely, the peak temperature T_0 and temperature gradient k_T. The inflow temperature linearly decreases with an increasing y-axis coordinate: $T = T_0 - k_T y$. A zero-temperature gradient corresponds to a uniform thermal condition, and an increase in k_T promotes the thermal stratification of reactants. According to the aforementioned formula, when the inflow temperature gradient, k_T, is 120 K/cm, the temperature T would reach 0 at $y = 10$ cm. This is not practical. To avoid such issues, we assume that when the fluid temperature is decreased to 300 K, it will not change further.

The initial parameters of the whole flow field are consistent with those of the left entrance and are supersonic in the laboratory frame; hence, supersonic outflow conditions are implemented on the right boundary, whose flow parameters can be extrapolated from the interior. The bottom boundary of the computational domain should be considered as a mirror symmetry plane on which the temperature is at peak value. Hence, the bottom of the computational domain is not a solid wall, and the boundary layer induced by walls does not need to be considered here. The vertical height of the computational domain is 0.3 m, which guarantees that the top boundary does not interact with the wave within the flow field. Accordingly, the top boundary of the computational domain is nonreflective. The horizontal size of the computational domain is 0.36 m, ensuring the completion of chemical reactions and the comprehensive development of detonation waves. To facilitate quantitative comparisons between the autoignition process and the detonation wave formation, a zoomed-in view of the local flow fields within the regions ($x = 0$–0.2 m and $y = 0$–0.1 m) are plotted in most figures.

A hypersonic airstream with a flight Mach number of 10 and an altitude of 30 km was considered. More details have been presented in the literature [18]. To simplify the choice of the inflow parameters, the inflow velocity U and pressure P were kept as integers, i.e., 2800 m/s and 150 kPa, respectively. The equivalence ratio ϕ of the H_2–air mixture was 1.0. Given the thermal nonuniformity induced by nonideal scenarios, the peak mixture temperature T_0 is likely to reach 1100–1300 K. As a representative case, a peak temperature T_0 of 1200 K was chosen to preset early autoignition and to reproduce a local high-temperature region in the domain. Furthermore, we adjusted the simulation domain length to ensure that the peak temperature (which is located on the bottom boundary of the computational domain) initiated autoignition at the location marked by a red dot in Fig 1. The effects of the peak temperature T_0 on autoignition morphology are also presented in the Supplemental Material [21].

Nonuniform distributions of the gas stream temperature in air-breathing engines usually form through the complex interactions of fuel jets and reflected shock waves. The chemical reaction rate is sensitive to temperature, and therefore, the irregular temperature profiles introduce substantial

uncertainties in the analysis of detonation initiation. Meanwhile, due to a lack of high-enthalpy wind tunnel capabilities, the temperature distributions have not been thoroughly confirmed through testing. For the time being, it is uncertain how temperatures are distributed in actual settings. In our simulations, only linear temperature profiles are presented in this study.

B. Governing equations and numerical approaches

Solving problems of hypersonic reactive flows requires a set of suitable governing equations coupled with a detailed chemical model. Assuming premixed and hypersonic flows, the species diffusion in detonation combustion can be ignored in most cases [22–25]. The viscous diffusion due to the velocity shear layer is also not considered here because the mainstream velocity in the horizontal direction greatly exceeds the transverse velocity. Additionally, previous studies [18,26,27] have found that the viscous diffusion hardly affects the large-scale wave structures, and the results obtained by solving the Euler and Navier-Stokes equations are basically similar for gaseous detonation waves. To assess the viscous effect, one typical case was solved using the Euler and Navier-Stokes equations. The simulation results are presented in the Supplemental Material [21]. It is seen that the viscous diffusion has little effect on the autoignition position and combustion wave structures. The chemistry is sensitive to the inflow temperature, and it is thus necessary to solve the rate equations of the full set of species to obtain correct characteristic chemical timescales. Hence, the Euler equations coupled with a multispecies reaction model are used to solve the hypersonic reactive flows:

$$\frac{\partial U}{\partial t} + \frac{\partial E}{\partial x} + \frac{\partial F}{\partial y} = S, \tag{1}$$

where

$$U = \begin{bmatrix} \rho_1 \\ \vdots \\ \rho_n \\ \rho u \\ \rho v \\ e \end{bmatrix}, \qquad E = \begin{bmatrix} \rho_1 u \\ \vdots \\ \rho_n u \\ \rho u^2 + p \\ \rho u v \\ (e+p)u \end{bmatrix}, \qquad F = \begin{bmatrix} \rho_1 v \\ \vdots \\ \rho_n v \\ \rho u v \\ \rho v^2 + p \\ (e+p)v \end{bmatrix}, \qquad S = \begin{bmatrix} \omega_1 \\ \vdots \\ \omega_n \\ 0 \\ 0 \\ 0 \end{bmatrix} \tag{2}$$

in which ρ, p, u, v, and e are the density, pressure, x velocity, y velocity, and specific total energy, respectively. ω in the source term represents the reaction rate of one specific species. The subscript index n is the number of all species.

The reaction model used in this work is a comprehensive H_2/O_2 mechanism [28]. It involves 27 reversible elementary reactions among eight species (H_2, O_2, H_2O, H, O, OH, HO_2, and H_2O_2) together with five inert species (N_2, Ar, He, CO, and CO_2). The thermodynamic properties of these species were evaluated using the nine-coefficient NASA polynomial formulas [29]. The solutions to the governing equations described above were numerically approximated using the second-order dispersion-controlled dissipation scheme [30] combined with a third-order Runge-Kutta algorithm [31]. In this study, the default grid scales were $\Delta x = \Delta y = 0.1$ mm. To verify grid convergence, the evolutions of basic results were examined at different grid scales. The grid scale used in this study is suitable for capturing the macrostructure of detonation waves but cannot reproduce the cellular structures on the wave front. The cellular structures on the surface of oblique detonation in high-temperature mixtures require a grid scale on the order of microns for resolution, which is too costly for engineering-scale combustor simulations. The resulting flow fields are presented and discussed in the Supplemental Material [21].
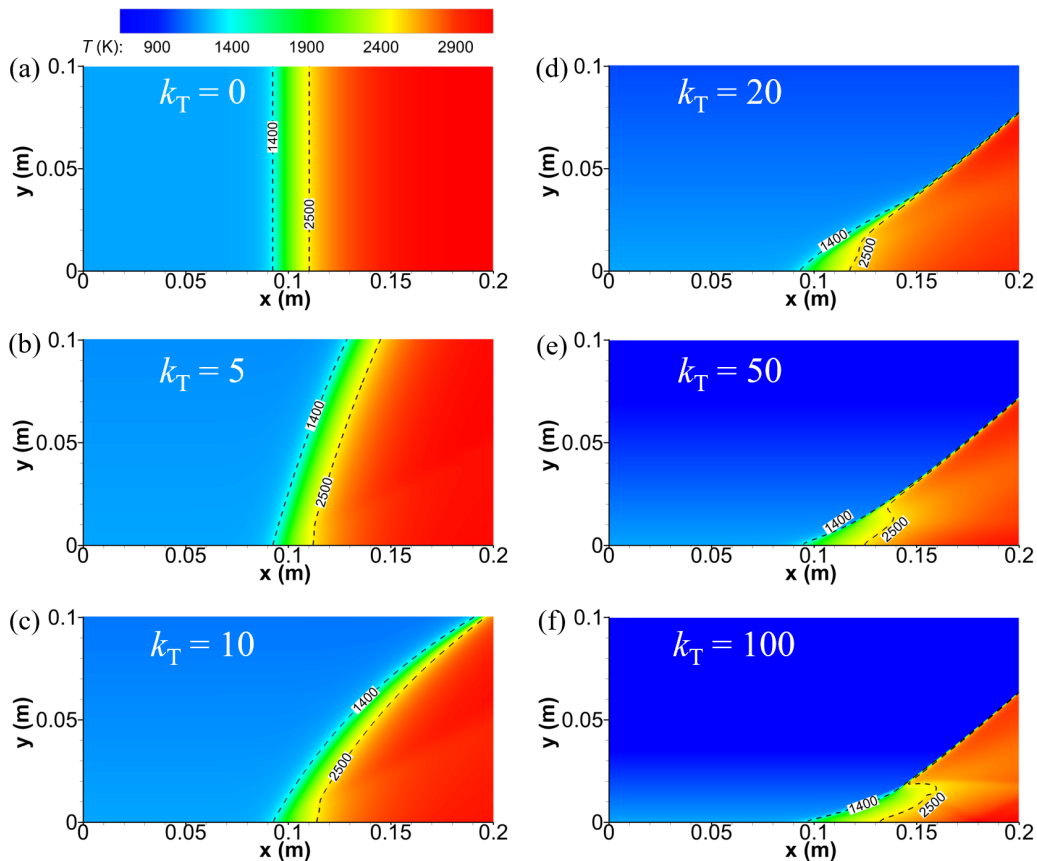
FIG. 2. Temperature fields with different temperature gradients. The dashed lines denote temperature isolines. The temperature gradient $k_T =$ (a) 0, (b) 5, (c) 10, (d) 20, (e) 50, and (f) 100 K/cm.

III. RESULTS AND DISCUSSIONS

A. Dependence of the wave morphology on temperature gradient

1. Flow fields with a low/moderate temperature gradient (0–100 K/cm)

Cases with different temperature gradients were simulated, and the corresponding temperature fields are shown in Fig. 2. For $k_T = 0$, where the inflow temperature is uniform, the autoignition occurs at about 0.1 m and the width of the heat release zone (green region) is approximately 0.02 m. The reaction front is perpendicular to the inflow. Increasing k_T to 5 K/cm causes an inclined reaction front owing to the low local temperature at a high position, but the width of the heat release zone is almost unchanged relative to that for uniform inflow. Although increasing k_T to 10 K/cm still does not change the local flow structure near $y = 0$, the width of the downstream heat release zone becomes narrow. This implies that the interaction of reactant stratifications with different temperatures is gradually acting.

At a temperature gradient of $k_T = 20$ K/cm, the downstream reaction front transforms into a new structure. Two key features are observed in Fig. 2(d). One is that the heat release zone forms tightly. The other is that the angle of the downstream reaction front remains almost constant, in contrast to the curved wave surface in Figs. 2(b) and 2(c). A similar phenomenon is observed in Figs. 2(e) and 2(f). The major difference among the cases is the morphology of the upstream reaction front in the region 0.1 m $< x <$ 0.15 m, where increasing k_T leads to a change from a convex to a concave wave
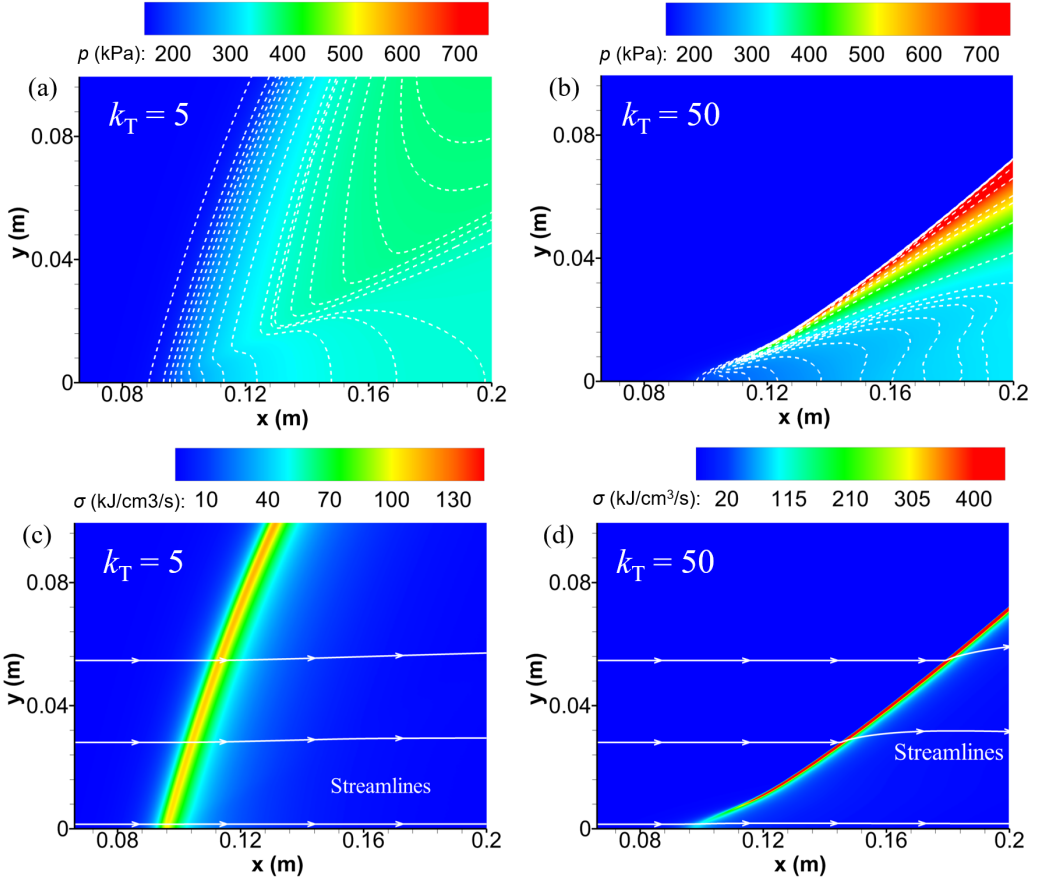
FIG. 3. Pressure (a), (b) and heat release rate (c), (d) fields for different temperature gradients k_T.

surface. More importantly, an increase in k_T has triggered a new combustion mode that is different from the upstream autoignition reaction front.

To examine the properties of the downstream reaction front, the pressure and heat release rate contours are shown in Fig. 3. Figure 3(a) shows that when k_T is 5 K/cm, the product pressure is approximately 350 kPa and is about 2.3 times that of the unburned mixture ($p = 150$ kPa). The pressure at the bottom boundary (along $y = 0$) is lower than that in the upper region owing to the local expansion. However, the pressure isolines narrow as y increases. The local heat release in supersonic flows generates a series of compression waves that compress the surrounding mixture. More compression waves propagate and converge downstream, finally narrowing the pressure isolines. For the case of $k_T = 50$ K/cm, there is a local high-pressure region along the reaction front and the pressure isolines are radially distributed in the high-pressure region.

The heat release rate fields in Figs. 3(c) and 3(d) show a remarkable difference in the exothermic layer width and peak rate. For $k_T = 5$ K/cm in Fig. 3(c), the width of the reaction zone is about 0.02 m and remains the same throughout the field. These autoignition phenomena are similar to those observed in previous studies [5,12,14], where the heat release mode in Fig. 3(c) is referred to as the autoignition-driven reaction front, which is dominated by the spatial distribution of the ignition delay times. Therefore, the heat release modes in Fig. 3(c) are different from the laminar burning flames driven by thermal and species transport processes. In Fig. 3(d), the streamlines across the downstream reaction front exhibit a slight deflection, indicating the presence of a nonzero
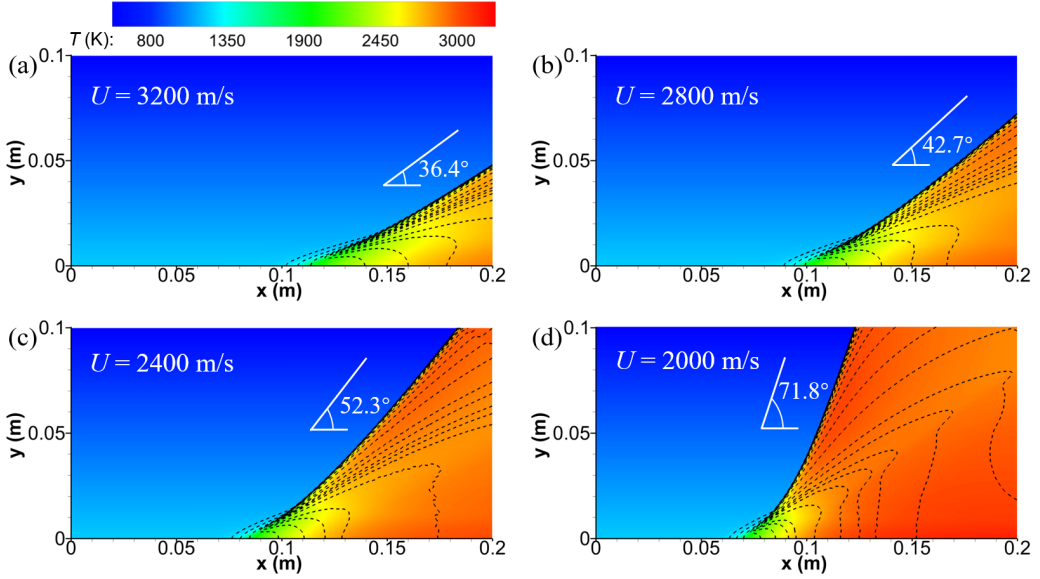
FIG. 4. Temperature fields and pressure isolines (black dashed lines) with a constant temperature gradient $k_T = 50$ K/cm and varying inflow velocities $U=$ (a) 3200 m/s, (b) 2800 m/s, (c) 2400 m/s, and (d) 2000 m/s. The white angle signs denote the prediction of the detonation propagation velocity using the Chapman-Jouguet criterion.

longitudinal velocity. The reaction zone width for $k_T = 50$ K/cm in Fig. 3(d) is about 0.003 m. The maximum rate of the downstream reaction front is on the order of 100 kJ cm^{-3} s^{-1}, whereas it is only approximately 100 kJ cm^{-3} s^{-1} at the upstream reaction front under the same inflows. Comparing Figs. 3(b) and 3(d), we observe that the downstream reaction front exhibits a sharp increase in pressure and a thin exothermic layer with a high reaction rate. This suggests the presence of a detonation wave in the downstream field in Figs. 2(d)–2(f).

An interesting phenomenon is that the detonation wave angles are almost the same in Figs. 2(d)–2(f). We next choose $k_T = 50$ K/cm as a base case and only change the inflow velocities to elaborate on the underlying mechanism. The temperature fields and pressure isolines are shown in Fig. 4. The angle marked on each map is a theoretical value defined according to the arcsine of the ratio of the one-dimensional (1D) Chapman-Jouguet (CJ) detonation speed V_{CJ} to the inflow velocity U, i.e., $\beta = \arcsin(V_{CJ}/U)$. The temperature of the unburned mixture varies in the range from 700 to 1200 K. Here, the mean temperature is used to predict V_{CJ}, which is approximately 1900 m/s. Figure 4 shows the behavior of the autoignition-detonation transition as the inflow velocity U changes from 3200 to 2000 m/s. The inflow velocity remarkably affects the downstream wave angle; i.e., the angle increases rapidly as the inflow velocity decreases. It is noted that the simulated wave angle is close to the theoretical angle drawn in white. In other words, the normal component of the horizontal inflow on the downstream wave surface equals the CJ speed of the premixed mixture, and the downstream detonation wave is in a near-CJ state.

Another phenomenon is that there exists a series of radial expansion waves behind the newly formed detonation wave, which is due to the deflection of horizontal flow behind the leading shock. The inflow direction is not perpendicular to the detonation wave, and the streamlines behind the oblique shock/detonation waves must have an anticlockwise deflection to satisfy the conservation laws. However, the longitudinal velocity component cannot remain the same because the downstream channel is horizontal, meaning that the downstream streams must experience a clockwise deflection through an expansion fan.
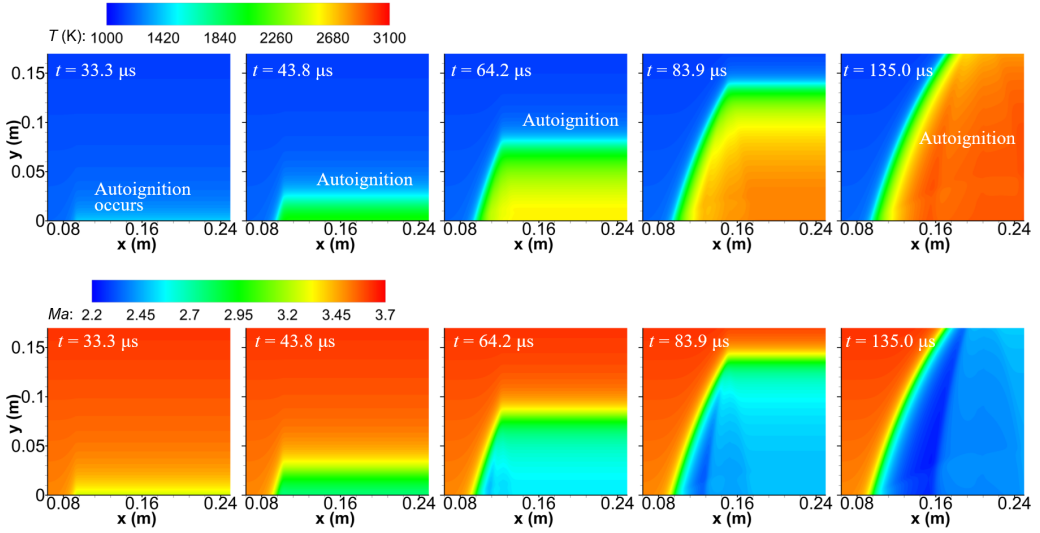
FIG. 5. Evolutions of local temperature (first row) and Mach number (second row) fields with temperature gradient $k_T = 5$ K/cm.

2. Formation processes of autoignition/detonation fronts

The steady-state fields of autoignition/detonation waves induced by temperature gradients were demonstrated in the previous section. This section selects two typical cases to demonstrate the formation process of autoignition/detonation fronts in hypersonic flows. Figure 5 displays the temperature (first row) and Mach number (second row) flow fields at different moments when the temperature gradient k_T is 5 K/cm. At $t = 33.3$ μs, the temperature at the bottom of the computational domain increases, and the Mach number decreases, indicating that autoignition has occurred. Additionally, a trapezoidal combustion zone can be observed within the flow field. As time progresses, the heat from chemical reaction gradually accumulates, not only expanding the area of the combustion zone but also increasing the temperature within it. The horizontal autoignition reaction front propagates vertically and passes through the upper boundary. The entire flow field presents a steady autoignition reaction front with a certain inclination angle. The Mach number flow field in the second row shows the same evolution process, but the Mach number within the combustion zone gradually decreases. This is mainly due to the increase in temperature, and it raises the sound speed of the local flow field.

As a contrast, Fig. 6 presents the temperature (first row) and Mach number (second row) fields at different moments for a temperature gradient of $k_T = 20$ K/cm. In the initial stage, $t < 43.8$ μs, the autoignition region is essentially the same as those observed with $k_T = 5$ K/cm. Subsequently, the evolution of the autoignition reaction front shows significant differences. For $k_T = 5$ K/cm, an autoignition reaction front is consistently present in the flow field. However, for $k_T = 20$ K/cm, the horizontal autoignition reaction front evolves into a detonation wave at $t = 64.2$ μs. Over time, the angle of the detonation wave gradually increases, which results in an oblique detonation wave that can be stabilized in hypersonic flows. The occurrence of autoignition increases the fluid temperature, leading to a decrease in the Mach number of the flow behind the reaction front. The formation of the detonation wave leads to a further decrease in Mach number. This is primarily due to the presence of a leading shock in front of the detonation wave, which compresses and slows down the fluid.

It is important to note that Figs. 5 and 6 present the initial stages of autoignition in the flow field, showcasing the transient characteristics. With the increase in the computational time, the resulting autoignition reaction fronts/detonation waves become steady, as shown in Fig. 2. The autoignition reaction front in Fig. 5 significantly differs from traditional low-speed flames. Typically, the flame
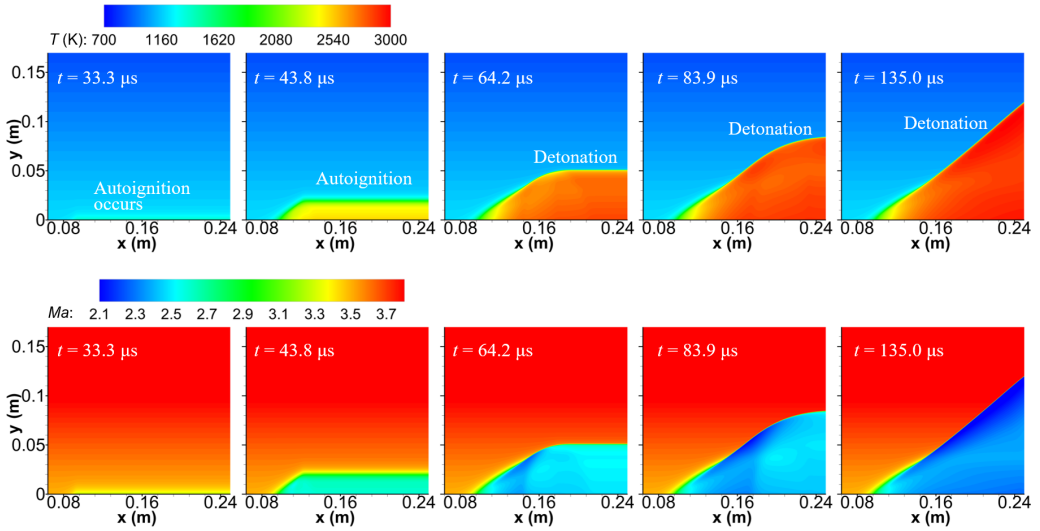
FIG. 6. Evolutions of local temperature (first row) and Mach number (second row) fields with temperature gradient $k_T = 20$ K/cm.

velocity depends on the transport processes of species/heat and it is generally less than 10 m/s [6–9]. Hence, the low-speed flame cannot remain stable in hypersonic flows. The reaction front in this study is induced by the autoignition process. The shape and location of the reaction fronts are mainly determined by the incoming flow velocity and the autoignition time of the reactants. These autoignition fronts are governed by the spatial distribution of reactant temperature and cannot be blown off. The oblique detonation wave in Fig. 6 can stabilize in hypersonic flows without any mechanical device, and is particularly interesting. The evolution process in Fig. 6 indicates that the upstream autoignition region provides an anchoring point. Once the detonation wave is initiated, as long as the normal velocity of the flow at the wave front matches the theoretical CJ detonation speed, the oblique detonation wave can achieve stabilization within hypersonic flow environments. This phenomenon is similar to projectile-induced detonation waves, wherein the projectile acts as the anchorage. In this study, the upstream autoignition zone serves as the anchorage point for the steady detonation waves.

3. Critical temperature gradients for detonation formation

The detonation development induced by thermal stratification has a minimum k_T, below which the heat release is achieved through the autoignition reaction. One ensuing question is whether there exists a maximum temperature gradient for the detonation formation. We further increased k_T, and the temperature fields for different temperature gradients are shown in Fig. 7. At $k_T = 120$ K/cm, the downstream reaction front is still a detonation wave. In contrast with the above-mentioned results in Fig. 2, the region connecting the upstream autoignition and downstream detonation is characterized by a multiwave point and not a smooth wave surface. This is similar to the smooth/abrupt patterns of wedge-induced oblique detonations, indicating a change in the mechanism of detonation initiation [32].

A further increase in k_T leads to the decoupling of shock wave and reaction front, as shown in Figs. 7(b) and 7(c). The downstream shock weakens and its compression capability is reduced; the post-shock temperature thus falls simultaneously. There is only one slender autoignition region near the bottom of the simulation domain. Although both large and small temperature gradients can result in autoignition reaction, they have different wave configurations. In the former case, the autoignition spreads over the downstream domain, and the reaction front is approximately perpendicular to
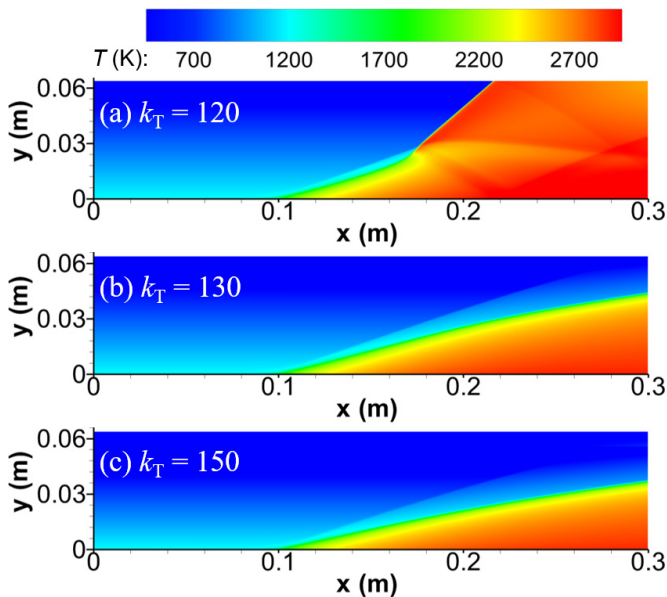
FIG. 7. Temperature fields for temperature gradients $k_T =$ (a) 120, (b) 130, and (c) 150 K/cm.

the horizontal inflow. In the latter case, the angle of the reaction front is decreased. Hence, only moderate k_T promotes the onset of the detonation wave. Beyond a specific temperature gradient range, only an autoignition reaction is observed in the flow field.

For the default inflow parameters in Sec. II A, the maximum k_T sustaining the formation of one detonation wave is in the range from 120 to 130 K/cm, where the peak temperature T_0 is 1200 K. The autoignition time mainly depends on the reactant temperature under a given pressure and equivalence ratio. We further examine the dependence of the critical temperature gradient on the peak temperature T_0, as shown in Fig. 8 (where the error bars extend ± 5 K/cm). It is noted that the development of autoignition-driven detonation in a one-dimensional channel has a minimum critical k_T that is usually less than 10 K/cm, but this does not meet the flow conditions of the air-breathing combustor, in which the temperature nonuniformity is approximately 100 K/cm. Hence, only the maximum k_T is presented in Fig. 8. When the peak temperature T_0 increases from 1100 to 1300 K,
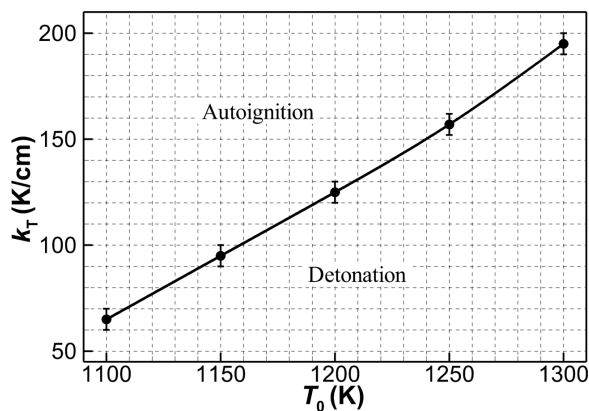

FIG. 8. Dependence of the critical temperature gradient on the peak temperature of the inflow.
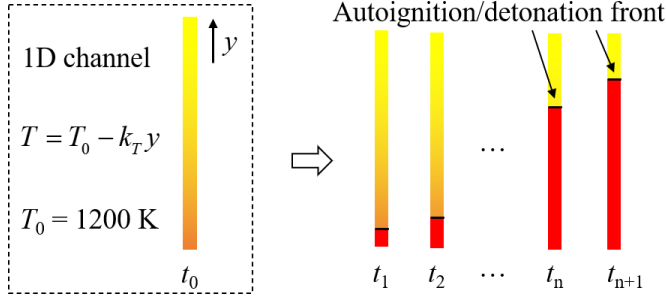
FIG. 9. Schematic of autoignition in a one-dimensional channel with a reactant temperature gradient.

the maximum critical temperature gradient that can trigger one detonation wave increases greatly. In other words, increasing the peak temperature T_0 is favorable to the formation of a detonation wave for a given temperature gradient. A greater T_0 corresponds to a greater inflow temperature and accelerates the induction reaction of reactants, and one detonation wave triggered by reactant thermal stratification is thus more easily obtained.

B. Role of horizontal flow in detonation formation

To clarify the effects of the hypersonic inflow on the development of mixture autoignitions, a one-dimensional unsteady autoignition is presented in this section. The 1D unsteady case is a reduced model in which the horizontal velocity in two-dimensional (2D) steady cases (obtained in Sec. III A) is not considered. Hence, the interactions between the horizontal flow and autoignition front are removed in the 1D case. Figure 9 is a schematic of autoignition/detonation development in a 1D channel with the same background temperature. The peak temperature T_0 is set to be 1200 K, and the initial temperature profile is calculated using the linear formula ($T = T_0 - k_T y$). The higher temperature at the bottom of the 1D channel first causes the reactant autoignition. The newly formed reaction front propagates along this channel, and finally, a detonation wave can form under appropriate temperature gradients.

The flow fields of 1D unsteady cases are shown in Fig. 10, where the horizontal axis indicates the time and each vertical profile denotes the flow field of the 1D channel at a certain moment t_n. When the mixture temperature is uniform, the autoignition of the whole field occurs concurrently. The result of the 1D case in Fig. 10(a) agrees well with that of the 2D case in Fig. 2(a). More importantly, the difference in the reaction front morphology is minimal for 1D and 2D results when $k_T \leqslant 10$ K/cm. The detonation development in 1D and 2D cases has a common mechanism, which is the amplification and interaction of pressure waves with chemical reactions [5,33,34]. However, there is a qualitative difference in the flow field for $k_T = 100$ K/cm. The 2D case considering the effects of horizontal flow can trigger a detonation, yet there is a decoupling of the leading shock and reaction front in the 1D case of Fig. 10(f). Hence, the supersonic flow can promote the formation of a detonation wave.

To quantitatively compare the differences between 1D and 2D reaction fronts, the 1D unsteady case should be transformed into pseudo 2D results represented in 2D (x,y) space. To achieve this objective, we assume that 1D cases have a horizontal velocity ($U = 2800$ m/s) that matches the inflow velocity of the 2D cases. By multiplying the time coordinate t in Fig. 10 by the horizontal velocity U, we can convert the results from a 2D (t,y) space to a 2D $(x = Ut,y)$ space. Subsequently, the reaction front is defined by the position of the beginning of the exothermic reaction, at which the gas temperature reaches 1.2 times the reactant temperature.

Figure 11 presents the morphology of the reaction front in the 1D and 2D cases. When $k_T = 10$ K/cm, the positions and shapes of these reaction fronts in Fig. 11(a) are essentially the same. The hypersonic inflow flow has little effect on the autoignition process for small thermal stratification.
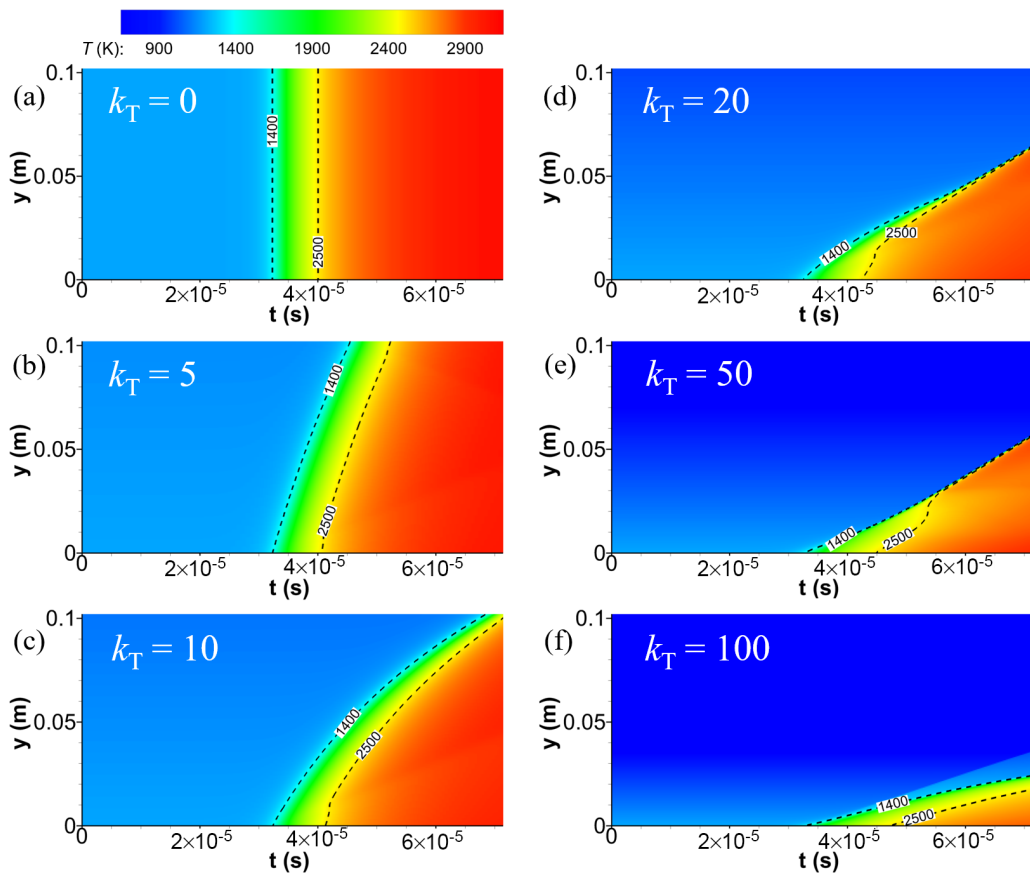
FIG. 10. Temperature fields of the one-dimensional channel at different instants for temperature gradient k_T = (a) 0, (b) 5, (c) 10, (d) 20, (e) 50, and (f) 100 K/cm. The dashed lines denote temperature isolines.

When k_T is increased to 20 K/cm, the differences between 1D and 2D results begin to emerge. Although the upstream reaction fronts in the various scenarios essentially overlap, the detonation initiation position in the 2D case is closer to the upstream and has a larger wave angle compared to the 1D case. Figure 11(c) illustrates similar phenomena for a temperature gradient of 50 K/cm, with the principal distinction being the angle of the reaction front.

Considering the presence of horizontal inflow in 2D cases, the interaction between the hypersonic flow and the reaction fronts further promotes detonation formation. The results in Figs. 11(b) and 11(c) demonstrate this point, where the detonation wave in 2D cases forms prior to that in 1D cases. Meanwhile, increasing k_T to 100 K/cm negatively affects the autoignition-to-detonation transition in the 1D cases, leading to a decoupling of shock wave and heat release. The angle of the reaction front marked by the black lines in Fig. 11(d) is about twice that in Fig. 11(c). However, if the horizontal inflow effects are considered in 2D simulations, the reaction front [red curve in Fig. 11(d)] for k_T = 100 K/cm still realizes the autoignition-to-detonation transition. The heat release in supersonic flows triggers a series of pressure waves, in which the mixture temperature is increased. Hence, the case of k_T = 100 K/cm in the 2D case with a hypersonic inflow can induce a detonation wave.

C. Discussion on detonation development

To ascertain how the reactant thermal stratification acts on detonation development, three typical cases with small (k_T = 5 K/cm), moderate (k_T = 20 K/cm), and large (k_T = 130 K/cm)
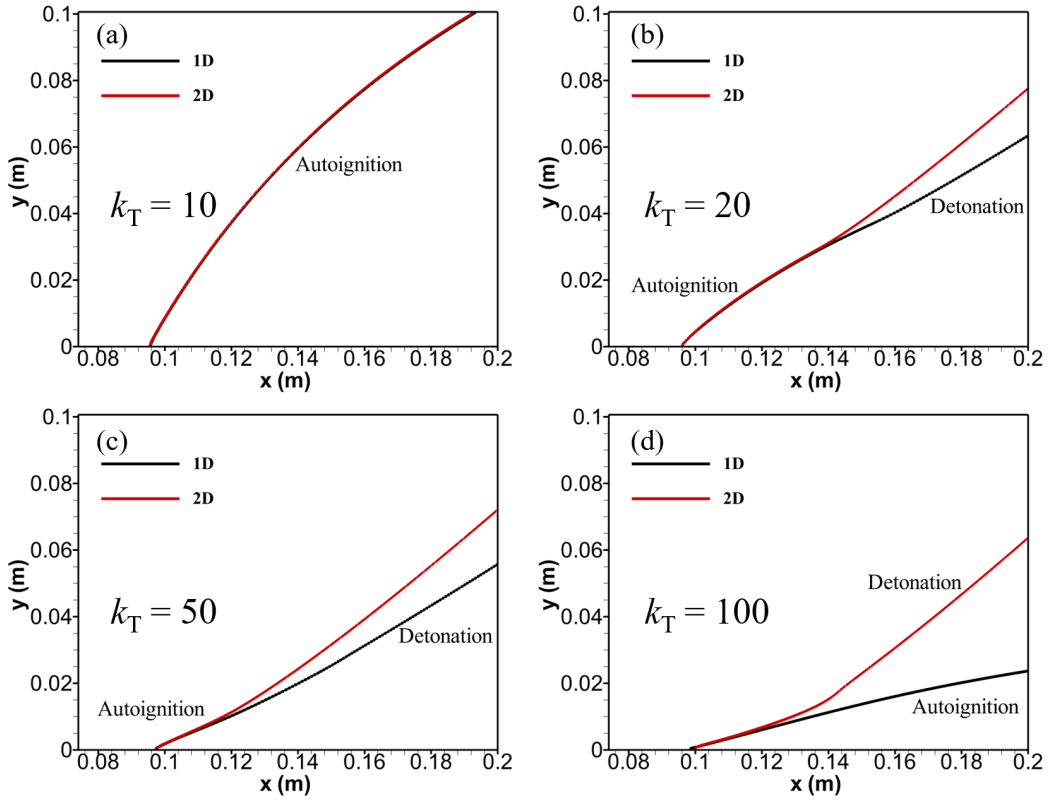
FIG. 11. Morphology of the reaction front in 1D and 2D cases for $k_T=$ (a) 10, (b) 20, (c) 50, and (d) 100 K/cm.

temperature gradients are chosen carefully. The corresponding pressure and heat release rate profiles along different lines parallel to the x axis are plotted in Fig. 12. For the autoignition process in Fig. 12(a), the exothermic reaction begins prior to the pressure jump. In other words, the local thermal expansion compresses the surrounding fluid particles and then increases the pressure. This autoignition regime is dominated by the reaction delay time, where the pressure profile slowly changes and the peak heat release rate is on the order of 100 kJ cm^{-3} s^{-1}. The detonation regime in Fig. 12(b) has a rapidly growing pressure profile in the early stage. The pressure wave is then coupled tightly with the heat release, and the two increase sharply and synchronously, meaning that a detonation wave forms downstream.

As a counterexample, the reaction front fails to couple with the leading shock for $k_T =$ 130 K/cm. Although the pressure profile in Fig. 12(c) has a sharp increase and the heat release rate behind the leading shock has a peak value ($\sim$100 kJ cm^{-3} s^{-1}), there is no detonation wave. Note that the pressure in Fig. 12(c) has a two-stage decrease. The first stage is located between the leading shock and reaction front, and the decrease in fluid pressure is due to the presence of an expansion wave induced by the streamline deflection. The second stage mainly relates to the thermal expansion derived from local heat release. More importantly, the distance between the shock front and the exothermic reaction front increases and the downstream heat release weakens.

The propagation characteristics of the reaction front play a greater role in detonation development. In previous studies [5,10,14], the propagation speed of the reaction front was found to be inversely proportional to the gradient of the reaction delay time. However, the autoignition wave in Fig. 2 is a steady structure. The propagation speed U_{RF} of the reaction front should be defined
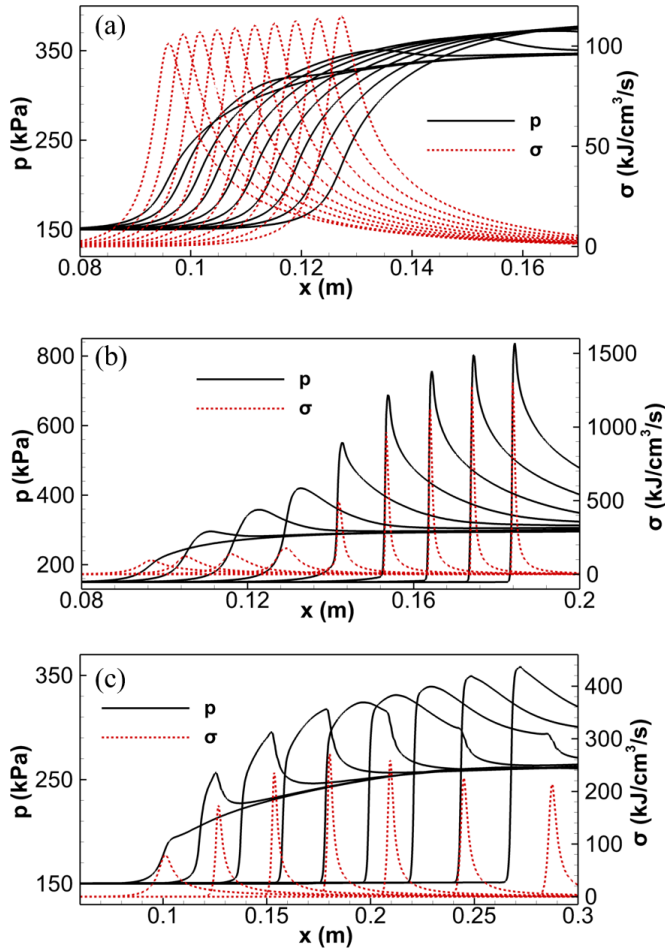
FIG. 12. Pressure and heat release rate profiles along different lines parallel to the x axis for temperature gradients k_T = (a) 5, (b) 20, and (c) 130 K/cm.

as the velocity component of incoming flow in the normal direction of the reaction front, as shown in Fig. 13. In the case of a low temperature gradient, the reaction front is only generated when the autoignition delay is reached. If the inflow velocity U is fixed, the propagation speed of the reaction
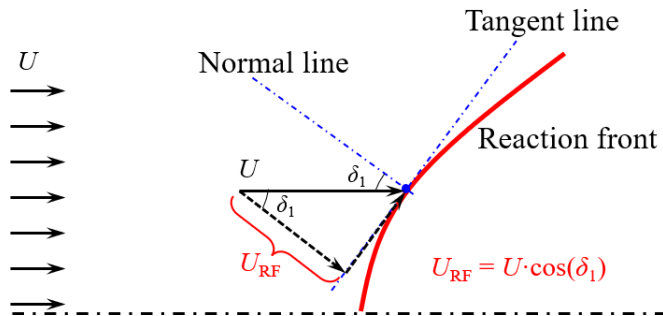

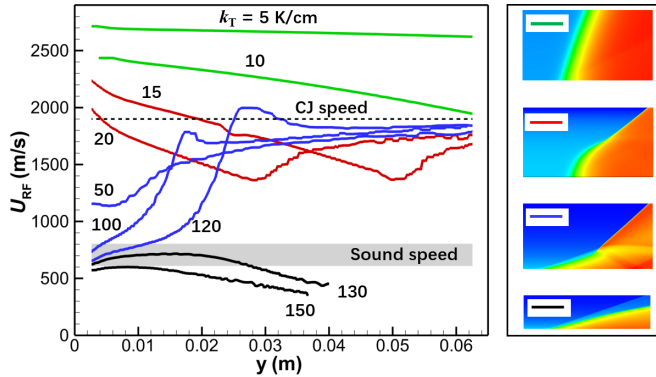FIG. 13. Propagation velocity of a two-dimensional steady reaction front.

FIG. 14. Propagation speed of the reaction front for linear temperature profiles.

front is dominated by the local curvature of the wave surface, which is not a constant in most cases. Hence, a larger wave angle denotes a higher speed of the steady reaction front.

To clarify the propagation properties of the reaction front during the autoignition-to-detonation transition, this work uses the unified term "reaction front wave speed" to refer to the propagation speed of the detonation wave and autoignition-driven reaction front. We further examine all simulated cases in this study and obtain the wave speeds of the reaction front presented in Fig. 14. Meanwhile, four local reaction-front morphologies are displayed in the right column to graphically illustrate the macroscopic differences among the typical flow structures with different inlet temperature profiles, showing two forms of autoignition and detonation. Note that the mixture temperature has little effect on the CJ speed, and the relative deviation is no greater than 2.5% for the temperature range from 700 to 1200 K. An average velocity (about 1900 m/s) predicted using the CJ criterion is marked by the dashed line in the figure. However, the temperature nonuniformity of the mixture always generates great variations in the local sound speed, which is marked by a gray region in the figure.

In Fig. 14, each wave speed curve has its own initial speed that is mainly determined by the temperature gradient (i.e., reaction delay time). A smaller k_T leads to a higher initial wave speed of the reaction front. However, the ensuing evolutions of these speed curves have large differences. At a small temperature gradient of $k_T = 5$ K/cm, the speed of the reaction front decreases slowly and is always higher than the CJ speed. A similar phenomenon is observed for $k_T = 10$ K/cm, where the wave speed monotonically decreases. If k_T is 130 K/cm (black lines), the wave speed of the reaction front first increases and then decreases gradually. The wave speed of the reaction front does not exceed the local sound speed, and a greater k_T further lowers the wave speed. It can be observed that a high or low wave speed is unable to induce a detonation wave through local autoignition.

However, the causes of these two failed autoignition-detonation transitions are different. A small k_T leads to a very fast reaction front whose wave speed is much greater than the local sound speed and even the CJ velocity. Meanwhile, the pressure disturbance induced by heat release theoretically propagates at the local sound speed. The pressure waves cannot converge prior to the reaction zone, and the leading shock for the detonation wave thus does not occur, as shown in Fig. 12(a). In the case of $k_T = 130$ K/cm, the leading shock forms, as shown in Fig. 12(c). However, the reaction-front wave speed cannot pass through the local sound speed region (see Fig. 14), and it falls continuously. The downstream reaction front cannot catch the forward pressure waves, and the amplification among these waves fades. The detonation wave cannot be obtained, and only a complex of the leading shock and reaction front can form in Fig. 12(c).

A slight decrease in k_T from 130 to 120 K/cm affects the evolution of the reaction-front wave speed. The speed curve for $k_T = 120$ K/cm slowly passes through the gray region of the sound

speed and then sharply increases and even overshoots the theoretical CJ speed. The reason is that the heat release during local autoignition generates pressure waves that propagate across the system. The unburned mixture behind the pressure wave might be compressed to react rapidly and, in turn, further enhance the pressure wave. Then, the compression waves and reaction front couple and one detonation wave forms. The acceleration of the reaction front behaves similarly at $k_T = 100$ and 50 K/cm. However, for $k_T = 15$ or 20 K/cm, the initial speed of the reaction front is usually greater than the CJ speed. The reaction front in the autoignition-detonation transition undergoes a deceleration-acceleration process. Detonation waves form in two ways. One way is the acceleration of the reaction front from the sound speed to the CJ speed. The other way is the deceleration-acceleration of the reaction front.

IV. CONCLUSIONS

Under the hypersonic flow conditions, the autoignition wave morphology induced by the thermal stratification of reactants was examined using the Euler equations coupled with a detailed chemical model for H_2-air mixtures. Three flow regimes, namely, the autoignition-driven reaction front, detonation wave, and decoupling shock/reaction front, were observed and confirmed under different inflow temperature profiles. For detonation development, there exists a critical temperature gradient that depends on the peak temperature of flow fields. Beyond the critical range, only an autoignition reaction begins to emerge. The effects of horizontal flow were analyzed systematically by introducing a 1D autoignition model. The presence of flows accelerates the autoignition-to-detonation transition because of the formation of pressure waves induced by the interactions of local thermal expansion and supersonic flow.

Although neither a small nor a large temperature gradient can induce a detonation wave, the underlying reasons are different. The former is due to the absence of pressure wave convergence, whereas the latter is due to the reaction fronts failing to catch up to the leading shock. Only moderate temperature gradients can trigger a detonation wave, where two preconditions of detonation development should be satisfied. First, the local autoignition induces a series of pressure waves, and their convergence is required. Second, the downstream reaction-front wave speed at the early stage should exceed the local sound speed, where the autoignition-driven reaction front interacts with the leading shock through acceleration or deceleration, mainly determined by the reaction-front wave speed at the initial stage. Consequently, the amplification between the leading shock and the reaction front occurs, leading to the formation of a fully developed detonation wave.

Our paper represents a preliminary exploration into nonuniform detonation research, focusing more on the types of wave patterns and their formation mechanisms while overlooking the impact of these flows on thrust performance. Based on the flow field results obtained so far, we are not yet able to analyze the engine thrust performance. Considering more realistic flow scenarios, the propulsion implications of these different flows will be a key focus of our future research. Furthermore, our study was conducted in an idealized context without considering the influence of other thermodynamic and geometric parameters, focusing primarily on whether temperature gradients can induce detonation waves. In future work, we plan to construct a more realistic geometric configuration and consider more practical flow scenarios, including nonuniformities in temperature, equivalence ratio, and velocity. Such flow scenarios are easier to achieve in high-enthalpy wind tunnels and will facilitate the validation of simulation results.

[1] P. Wolański, Detonative propulsion, Proc. Combust. Inst. **34**, 125 (2013).

[2] J. Urzay, Supersonic combustion in air-breathing propulsion systems for hypersonic flight, Annu. Rev. Fluid Mech. **50**, 593 (2018).

[3] V. Anand and E. Gutmark, Rotating detonation combustors and their similarities to rocket instabilities, Prog. Energy Combust. Sci. **73**, 182 (2019).

[4] K. Wang, H. Teng, P. Yang, and H. D. Ng, Numerical investigation of flow structures resulting from the interaction between an oblique detonation wave and an upper expansion corner, J. Fluid Mech. **903**, A28 (2020).

[5] X. J. Gu, D. R. Emerson, and D. Bradley, Modes of reaction front propagation from hot spots, Combust. Flame **133**, 63 (2003).

[6] G. J. Sharpe and M. Short, Detonation ignition from a temperature gradient for a two-step chain-branching kinetics model, J. Fluid Mech. **476**, 267 (2003).

[7] P. Dai, Z. Chen, and X. Gan, Autoignition and detonation development induced by a hot spot in fuel-lean and CO_2 diluted n-heptane/air mixtures, Combust. Flame **201**, 208 (2019).

[8] D. Yu and Z. Chen, Theoretical analysis on the ignition of a combustible mixture by a hot particle, J. Fluid Mech. **936**, A22 (2022).

[9] D. Yu and Z. Chen, Theoretical analysis on the transient ignition of a premixed expanding flame in a quiescent mixture, J. Fluid Mech. **924**, A22 (2021).

[10] Y. B. Zel'dovich, Regime classification of an exothermic reaction with nonuniform initial conditions, Combust. Flame **39**, 211 (1980).

[11] A. Robert, S. Richard, O. Colin, and T. Poinsot, LES study of deflagration to detonation mechanisms in a downsized spark ignition engine, Combust. Flame **162**, 2788 (2015).

[12] L. Bates and D. Bradley, Deflagrative, auto-ignitive, and detonative propagation regimes in engines, Combust. Flame **175**, 118 (2017).

[13] P. Dai, Z. Chen, X. Gan, and M. A. Liberman, Autoignition and detonation development from a hot spot inside a closed chamber: Effects of end wall reflection, Proc. Combust. Inst. **38**, 5905 (2021).

[14] Y. Gao, P. Dai, and Z. Chen, Numerical studies on autoignition and detonation development from a hot spot in hydrogen/air mixtures, Combust. Theor. Model. **24**, 245 (2020).

[15] D. C. Alexander and J. P. Sislian, Computational study of the propulsive characteristics of a shcramjet engine, J. Propul. Power **24**, 34 (2008).

[16] C. Huete, A. L. Sánchez, F. A. Williams, and J. Urzay, Diffusion-flame ignition by shock-wave impingement on a supersonic mixing layer, J. Fluid Mech. **784**, 74 (2015).

[17] Z. Zhang, K. Ma, W. Zhang, X. Han, Y. Liu, and Z. Jiang, Numerical investigation of a Mach 9 oblique detonation engine with fuel pre-injection, Aerosp. Sci. Technol. **105**, 106054 (2020).

[18] H. Teng, C. Tian, Y. Zhang, L. Zhou, and H. D. Ng, Morphology of oblique detonation waves in a stoichiometric hydrogen–air mixture, J. Fluid Mech. **913**, A1 (2021).

[19] L. Yang, L. Yue, Q. Zhang, and X. Zhang, Numerical study on the shock/combustion interaction of oblique detonation waves, Aerosp. Sci. Technol. **104**, 105938 (2020).

[20] P. Yang, H. D. Ng, H. Teng, and Z. Jiang, Initiation structure of oblique detonation waves behind conical shocks, Phys. Fluids **29**, 086104 (2017).

[21] See Supplemental Material at http://link.aps.org/supplemental/10.1103/PhysRevFluids.9.083202 for the effects of viscosity, grid scale, and inflow temperature/pressure on the wave patterns in the flow field. It also presents the Zel'dovich–von Neumann–Döring (ZND) structure of one-dimensional detonation waves under high-static-temperature conditions.

[22] P. Yang, H. D. Ng, and H. Teng, Numerical study of wedge-induced oblique detonations in unsteady flow, J. Fluid Mech. **876**, 264 (2019).

[23] H. Teng, Y. Zhang, and Z. Jiang, Numerical investigation on the induction zone structure of the oblique detonation waves, Comput. Fluids **95**, 127 (2014).

[24] V. N. Gamezo, D. Desbordes, and E. S. Oran, Formation and evolution of two-dimensional cellular detonations, Combust. Flame **116**, 154 (1999).

[25] W. Han, W. Kong, Y. Gao, and C. K. Law, The role of global curvature on the structure and propagation of weakly unstable cylindrical detonations, J. Fluid Mech. **813**, 458 (2017).

[26] K. Mazaheri, Y. Mahmoudi, and M. I. Radulescu, Diffusion and hydrodynamic instabilities in gaseous detonations, Combust. Flame **159**, 2138 (2012).

[27] X. Xi, H. Teng, Z. Chen, and P. Yang, Effects of longitudinal disturbances on two-dimensional detonation waves, Phys. Rev. Fluids **7**, 043201 (2022).

[28] M. P. Burke, M. Chaos, Y. Ju, F. L. Dryer, and S. J. Klippenstein, Comprehensive H_2/O_2 kinetic model for high-pressure combustion, Int. J. Chem. Kinet. **44**, 444 (2012).

[29] B. J. Mcbride, M. J. Zehe, and S. Gordon, NASA Glenn Coefficients for Calculating Thermodynamic Properties of Individual Species, NASA Technical Report No. 2002-211556, NASA Glenn Research Center, Cleveland, Ohio, 2000.

[30] Z. Jiang, Dispersion-controlled principles for non-oscillatory shock-capturing schemes, Acta Mech. Sin. **20**, 1 (2004).

[31] K. H. Kim, C. Kim, and O.-H. Rho, Methods for the accurate computations of hypersonic flows: I. AUSMPW+ scheme, J. Comput. Phys. **174**, 38 (2001).

[32] H. H. Teng and Z. L. Jiang, On the transition pattern of the oblique detonation structure, J. Fluid Mech. **713**, 659 (2012).

[33] J. H. Lee, *The Detonation Phenomenon* (Cambridge University Press, Cambridge, 2008).

[34] J. H. Lee, R. Knystautas, and N. Yoshikawa, Photochemical initiation of gaseous detonations, Acta Astronaut. **5**, 971 (1978).